Ortho-Metalated Ruthenium Hydrido Dihydrogen Complexes: Dynamics, Exchange Couplings, and Reactivity

Jochen Matthes,[†,‡] Stephan Gründemann,[†] Andrew Toner,[‡] Yannick Guari,[‡] Bruno Donnadieu,[‡] Johann Spandl,[†] Sylviane Sabo-Etienne,*[,‡] Eric Clot,*[,§] Hans-Heinrich Limbach,*[,†] and Bruno Chaudret*[,‡]

Institute of Chemistry, Freie Universität Berlin, Takustrasse 3, D-14195 Berlin, Germany, Laboratoire de Chimie de Coordination du CNRS, Université Paul Sabatier, 205 route de Narbonne, 31077 Toulouse Cedex 04, France, and Laboratoire de Structure et Dynamique des Systèmes Moléculaires et Solides (UMR 5636), case courrier 14, Université Montpellier II, Place Eugène Bataillon, 34905 Montpellier Cedex, France

Received October 24, 2003

A series of ortho-metalated ruthenium hydrido dihydrogen complexes of the form RuH(H_2)(X)(P^iPr_3)$_2$ (X = 2-phenylpyridine (ph-py) (**2**), benzoquinoline (bq) (**3**), phenylpyrazole (ph-pz) (**4**)) were prepared by adding 1 equiv of the corresponding substrate X−H and 2 equiv of P^iPr_3 to Ru(COD)(COT) under 3 bar of H_2. The analogous complex RuH(H_2)(ph-py)(PCy_3)$_2$ (**1**) was prepared by adding 1 equiv of 2-phenylpyridine to RuH$_2$(H_2)$_2$(PCy_3)$_2$. The ortho-metalated X ligand is coordinated to ruthenium via the nitrogen of one ring and the ortho carbon of a second ring as a result of C−H activation. **2** and **3** were characterized by X-ray diffraction. They are the first examples of complexes displaying exchange couplings between the hydride and the dihydrogen ligands. NMR studies and DFT calculations are used to understand this phenomenon. The series of ortho-metalated model complexes RuH(H_2)(X)(PH_3)$_2$ was investigated by DFT at the B3PW91 level. The coherent (quantum-mechanical) as well as the incoherent (classical) exchange rates have been determined by line shape analysis, and the activation energies hardly depend on the nature of the X ligand: E_a(coherent) = ca. 10 kJ mol^{-1}, E_a(incoherent) = ca. 40 kJ mol^{-1} (ca. 50 kJ mol^{-1} by DFT). The corresponding transition states (**2q**$^{\mathbf{TSQEC}}$−**4q**$^{\mathbf{TSQEC}}$) for the classical exchange process have been located by DFT at the B3PW91 level. The dihydrogen ligand is now trans to N and perpendicular to the plane of the chelating ligand. These states connect to the isomer with the dihydrogen trans to C through coupled rotation of H_2 and proton transfer from H_2 to H. The dihydrogen ligand can be substituted easily, and the corresponding complexes RuH(L)(ph-py)(P^iPr_3)$_2$ with L = N_2 (**5**), O_2 (**6**), CO (**7**), C_2H_4 (**8**) have been isolated and fully characterized by NMR and by crystal structure analyses in the case of **6** and **8**. The model systems RuH(L)(ph-py)(PH_3)$_2$ (**5q**−**8q**) have been optimized at the DFT level (B3PW91). In the case of **8**, we could not detect any ethylene insertion in either the Ru−H or the Ru−C bond. Theoretical calculations explain the differences we observed with the Murai type catalysts, which are highly reactive to ethylene insertion.

Introduction

The functionalization of C−H bonds is a problem of both academic and industrial importance.[1] Different routes have been presently explored for achieving this goal catalytically by using molecular transition-metal catalysts. They include early transition metals and electrophilic or nucleophilic systems with late transition metals.[2] In this context, the system extensively developed by Murai's group represents a very interesting example of such catalysis.[3] C−C bond coupling of an olefin with a functionalized aromatic compound is achieved by chelating assistance, allowing ortho C−H bond cleavage. Some of us have already shown that the ortho-metalated ruthenium complexes RuH(H_2)(*o*-C_6H_4-COR)(PCy_3)$_2$ (R = Me, Ph) resulting from C−H bond activation of an arene ketone can indeed be isolated and used as catalyst precursors for the ethylene insertion into the ortho C−H bond of acetophenone or benzophenone at room temperature.[4] The presence of an η^2-dihydrogen ligand in the complex may be at the origin

* To whom correspondence should be addressed. E-mail: sabo@lcc-toulouse.fr (S.S.-E.).
† Freie Universität Berlin.
‡ Université Paul Sabatier.
§ Université Montpellier II.

(1) Labinger, J. A.; Bercaw, J. E. *Nature* **2002**, *417*, 507.
(2) (a) Jia, C.; Kitamura, T.; Fujiwara, Y. *Acc. Chem. Res.* **2001**, *34*, 633. (b) Ritleng, V.; Sirlin, C.; Pfeffer, M. *Chem. Rev.* **2002**, *102*, 1731. (c) Guari, Y.; Sabo-Etienne, S.; Chaudret, B. *Eur. J. Inorg. Chem.* **1999**, 1047. (d) Dyker, G. *Angew. Chem., Int. Ed. Engl.* **1999**, *38*, 1698.
(3) (a) Murai, S.; Kakiuchi, F.; Sekine, S.; Tanaka, Y.; Kamatani, A.; Sonoda, M.; Chatani, W. *Nature* **1993**, *366*, 529. (b) Kakiuchi, F.; Murai, S. *Acc. Chem. Res.* **2002**, *35*, 826.
(4) (a) Guari, Y.; Sabo-Etienne, S.; Chaudret, B. *J. Am. Chem. Soc.* **1998**, *120*, 4228. (b) Guari, Y.; Castellanos, A.; Sabo-Etienne, S.; Chaudret, B. *J. Mol. Catal.*, in press.

10.1021/om034259c CCC: $27.50
Publication on Web 02/14/2004

Table 1. Crystal Data for 2, 3, 6, and 8

	2	3	6	8
chem formula	$C_{29}H_{50}NP_2Ru$	$C_{31}H_{53}NP_2Ru$	$C_{29}H_{51}NO_2P_2Ru$	$C_{31}H_{55}NP_2Ru$
formula wt	575.71	602.75	608.72	604.77
cryst syst	orthorhombic	triclinic	monoclinic	triclinic
space group	*Pbcn*	$P\bar{1}$	$P2_1/n$	$P\bar{1}$
Z; calcd density, Mg/m^3	4; 1.297	2; 1.319	4; 1.306	2; 1.282
abs coeff, mm^{-1}	0.657	0.642	0.634	0.622
F(000)	1220	640	1288	644
a, Å	8.6468(13)	10.214(3)	12.251(3)	9.8610(6)
b, Å	19.014(3)	10.919(3)	19.468(3)	10.3982(6)
c, Å	17.927(3)	14.553(4)	13.042(4)	16.2667(10)
α, deg		85.05(3)		80.7480(10)
β, deg		76.78(3)	95.54(3)	84.8190(10)
γ, deg		73.85(3)		72.3510(10)
V, Å^3	2947.4(8)	1517.3(7)	3096.0(12)	1567.22(16)
temp, K	150(2)	113(2)	180(2)	183(2)
no. of data/restraints/params	2332/0/156	4513/0/340	4821/0/332	8962/0/349
goodness of fit on F^2	1.231	1.150	1.053	1.070
R1 ($I > 2\sigma(I)$)	0.0374	0.0304	0.0305	0.0238
wR2	0.0925	0.0737	0.0583	0.0581
largest diff peak and hole, e Å^{-3}	0.689 and −0.462	0.439 and −0.398	0.312 and −0.359	0.457 and −0.250

of the ease of this reaction. In an attempt to gain better knowledge of the mechanism of C−H activation and carbon−carbon bond formation in such compounds, we have undertaken a systematic study of hydrogen exchange in these and related systems. We have already published preliminary results on the hydrido dihydrogen complexes $RuH(H_2)(ph\text{-}py)(PR_3)_2$ (R = Cy (**1**), ^{i}Pr (**2**); ph-py = *o*-$C_6H_4C_5H_4N$), containing an ortho-metalated phenylpyridyl ligand, and shown that protonation leads to a complex accommodating a dihydrogen ligand and a weak agostic C−H bond in equilibrium with a dihydrogen ortho-metalated complex.[5]

We now report the full characterization of compounds **1** and **2** and of derivatives similar to **2** but containing metalated 7,8-benzoquinoline (bq) or 1-phenylpyrazole (ph-pz). The dynamics of the hydrogens (hydride and dihydrogen ligand) present in the coordination sphere of the metal are described in each case, by combining NMR studies and DFT calculations. Moreover, we show that the dihydrogen ligand in **2** is easily substituted, as illustrated by the reactivity of **2** with ethylene, dioxygen, dinitrogen, and carbon monoxide.

Results and Discussion

Synthesis and Properties of Neutral Hydrido Dihydrogen Ortho-Metalated Complexes. The reaction of $RuH_2(H_2)_2(PCy_3)_2$[6] with phenylpyridine (H-ph-py) affords the metalated species $RuH(H_2)(ph\text{-}py)(PCy_3)_2$ (**1**). Complex **1** was found to be insufficiently soluble for full NMR characterization and recrystallization. We thus looked for an alternative preparation leading to a similar but more soluble derivative. We chose to use P^{i}Pr$_3$ as an ancillary ligand and reacted in one pot Ru(COD)(COT) (COD = 1,5-C_8H_{12}; COT = 1,3,5-C_8H_{10}) with 1 equiv of H-ph-py and 2 equiv of P^{i}Pr$_3$ in pentane under 3 bar of dihydrogen. The product, $RuH(H_2)(ph\text{-}py)(P^iPr_3)_2$ (**2**), was shown to display spectroscopic features very similar to those of **1**. The corresponding benzoquinoline (H-bq) and 1-phenylpyrazole (H-ph-pz) complexes, namely $RuH(H_2)(bq)(P^iPr_3)_2$ (**3**) and $RuH(H_2)(ph\text{-}pz)(P^iPr_3)_2$ (**4**) (see Chart 1), were also prepared in the same way.

Chart 1. Structures of Ortho-Metalated Hydrido Dihydrogen Complexes 2−4 and Numbering of Protons and Carbons in the Ligands

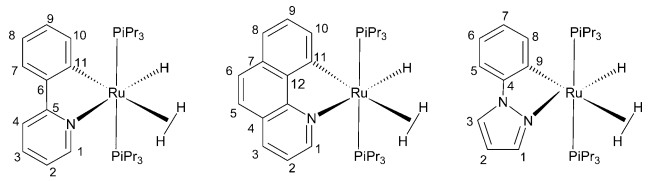

The new complexes **1**−**4** were characterized by microanalysis and NMR data. Their full characterization is given in the Experimental Section. Complexes **2** and **3** were also characterized by X-ray analysis (see Tables 1 and 2). The complexes display a distorted-octahedral environment with two trans phosphine ligands (P−Ru−P angle ca. 165°) and, in the equatorial plane, the metalated ligand (ph-py for **2** and bq for **3**). The hydride and dihydrogen ligands were located in the case of **3** (see Figure 1). In the case of **2**, some disorder prevented the localization of the carbon and the nitrogen atoms bound to the ruthenium and thus the localization of the hydrides.

Localization of hydrogen atoms by X-ray measurements[7] is always subject to debate, and in the field of polyhydride chemistry, computational studies have proved to be a very efficient means to obtain structural information and, particularly, to locate hydrides securely.[8] We have thus carried out DFT calculations (B3PW91) on the model systems $RuH(H_2)(ph\text{-}py)(PH_3)_2$ (**2q**), $RuH(H_2)(bq)(PH_3)_2$ (**3q**; see Figure 1), and $RuH(H_2)(ph\text{-}pz)(PH_3)_2$ (**4q**), where the only simplification lies in the nature of the phosphine ligand. For the phenylpyridine complex **2q**, the calculated geometry (Table 2) confirms the presence of a dihydrogen ligand trans to the ortho-metalated C (with a H(2)−H(3) bond distance of 0.905 Å). Due to the hydride cis effect,[9] the Ru−H(3) bond distance is shorter than the Ru−H(2)

(5) Toner, A. J.; Gründemann, S.; Clot, E.; Limbach, H.-H.; Donnadieu, B.; Sabo-Etienne, S.; Chaudret, B. *J. Am. Chem. Soc.* **2000**, *122*, 6777.

(6) (a) Sabo-Etienne, S.; Chaudret, B. *Coord. Chem. Rev.* **1998**, *178*−*180*, 381. (b) Borowski, A. F.; Sabo-Etienne, S.; Christ, M. L.; Donnadieu, B.; Chaudret, B. *Organometallics* **1996**, *15*, 1427. (c) Borowski, A. F.; Donnadieu, B.; Daran, J.-C.; Sabo-Etienne, S.; Chaudret, B. *Chem. Commun.* **2000**, 543.

(7) Zhao, D.; Bau, R. *Inorg. Chim. Acta* **1998**, *269*, 601.

(8) (a) Maseras, F.; Lledós, A.; Clot, E.; Eisenstein, O. *Chem. Rev.* **2000**, *100*, 601. (b) Atheaux, I.; Delpech, F.; Donnadieu, B.; Sabo-Etienne, S.; Chaudret, B.; Hussein, K.; Barthelat, J.-C.; Braun, T.; Duckett, S. B.; Perutz, R. N. *Organometallics* **2002**, *21*, 5347.

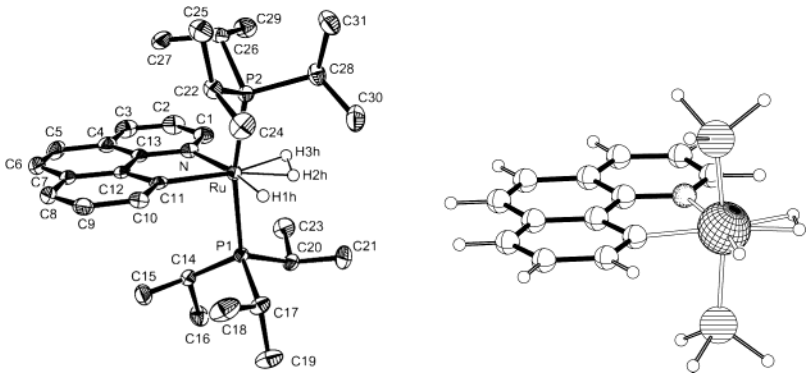

Figure 1. X-ray crystal structure of $RuH(H_2)(bq)(P^iPr_3)_2$ (**3**) and calculated structure for the model system $RuH(H_2)(bq)(PH_3)_2$ (**3q**).

Table 2. Selected Bond Distances (Å) and Angles (deg) for the Three Molecular Dihydrogen Complexes (2q, 3q, and 4q) and the Corresponding Transition States for Classical H/H_2 Exchange ($2q^{TSQEC}$, $3q^{TSQEC}$, and $4q^{TSQEC}$) Optimized at the B3PW91 Level with the Calculated Activation Energy $\Delta E^{\ddagger}$ (kJ mol^{-1}) and Comparison with the X-ray Data of 2 and 3

	2 (X-ray)	**2q**	$\mathbf{2q^{TSQEC}}$	**3** (X-ray)	**3q**	$\mathbf{3q^{TSQEC}}$	**4q**	$\mathbf{4q^{TSQEC}}$
Ru−H(1)		1.609	1.693	1.54(4)	1.605	1.689	1.606	1.686
Ru−H(2)		1.728	1.687	1.57(5)	1.726	1.682	1.723	1.674
Ru−H(3)		1.700	1.693	1.68(4)	1.697	1.689	1.700	1.686
H(1)−H(2)		1.977	0.877	1.75(6)	1.968	0.880	1.987	0.881
H(2)−H(3)		0.905	2.401	0.82(6)	0.905	2.406	0.903	2.373
Ru−C	2.135(3)	2.063	2.094	2.104(3)	2.069	2.106	2.073	2.117
Ru−N	2.135(3)	2.174	2.086	2.155(3)	2.192	2.095	2.163	2.064
Ru−P	2.3392(8)	2.293	2.298	2.3562(11) 2.3334(11)	2.293	2.298	2.294	2.302
P−Ru−P	165.65(4)	165.2	163.4	164.51(3)	165.9	163.5	164.4	165.6
$\Delta E^{\ddagger}$		55.7			53.4		54.5	

distance (1.700 vs 1.728 Å), but the computed H(1)···H(2) distance of 1.977 Å is too long for a bonding interaction. For **2q**, no local minimum with H_2 trans to N could be located on the potential energy surface. All attempts yielded the dihydrogen complex with H_2 trans to C. This reflects the unfavorable situation of two strong σ-donor groups mutually trans (C and H). This bonding pattern is also observed for **3q** (**4q**), where the H_2 ligand trans to C has an H−H bond distance of 0.905 Å (0.903 Å). As shown in Table 2, the geometries around the transition-metal center are very similar for the three complexes **2q**−**4q**. This may explain their similar spectroscopic behavior.

The most salient spectroscopic feature of compounds **1**−**4** is the presence at room temperature of a high-field peak in the ^{1}H NMR spectrum integrated for three protons and corresponding to the hydride and dihydrogen ligands in exchange near −8.5 ppm for complexes **1**−**3** and at −9.2 ppm for complex **4**. The ortho-metalated ligand is predominantly characterized by low-field doublets for H1 and H10 between 8 and 10 ppm (the corresponding proton in complex **4** being H8). The remaining signals have chemical shifts and multiplicities similar to those of the uncoordinated ligand. In the $^{31}P\{^1H\}$ NMR spectrum, a single signal is observed for the two equivalent trans phosphorus atoms at 46 ppm for the bis(tricyclohexylphosphine) complex **1** and near 58 ppm for the bis(triisopropylphosphine) complexes **2**−**4**. In the ^{13}C NMR spectra, the most salient characteristic is the ortho-metalated carbon resonance. It appears as a triplet shifted to 197, 195, and 176 ppm in complexes **2**−**4**, respectively, with a $^2J_{CP}$ coupling of 11 Hz. In addition, NMR investigations between 293 and 163 K in THF-d_8 solutions demonstrate the presence of both quantum-mechanical (coherent)[10] and classical (incoherent) exchange processes between the hydrogen atoms present in the coordination sphere of complexes **2**−**4**. The superimposed experimental and calculated spectra of the hydride region at selected temperatures are shown in Figure 2. The spectra are similar for all three complexes. At room temperature a single line is observed for all three hydrogen nuclei. As the temperature is decreased, this line broadens and splits into a doublet and triplet due to an AB_2 spin system displaying unusually large H−H coupling constants (between 300 and 400 Hz at 213 K) resulting from quantum-mechanical exchange. At 183 K, the triplet changes into a triplet of triplets as coupling to the two equivalent phosphorus atoms is resolved. As the two hydrogen atoms in the dihydrogen ligand are magnetically equivalent, the line shape in the ^{1}H NMR spectra depends on the chemical shifts ν_1 and ν_2 of the two hydrogen sites, corresponding respectively to the hydride and the dihydrogen ligands, the exchange coupling J_{12} between the hydride and the dihydrogen ligand, and the rate constant k_{12}. Furthermore, the scalar coupling constant of the hydride ligand with the two magnetically equivalent phosphorus atoms J_{HP} is resolved at lower temperatures. The scalar coupling between the protons of the dihydrogen ligand and the phosphorus atoms was not resolved and therefore neglected. The relaxation time T_1 values are given in the Experimental Section and are in agreement with the presence of a dihydrogen ligand.

(9) Van der Sluys, L. S.; Eckert, J.; Eisenstein, O.; Hall, J. H.; Huffman, J. C.; Jackson, S. A.; Koetzle, T. F.; Kubas, G. J.; Vergamini, P. J.; Caulton, K. G. *J. Am. Chem. Soc.* **1990**, *112*, 4831.

(10) Sabo-Etienne, S.; Chaudret, B. *Chem. Rev.* **1998**, *98*, 2077.

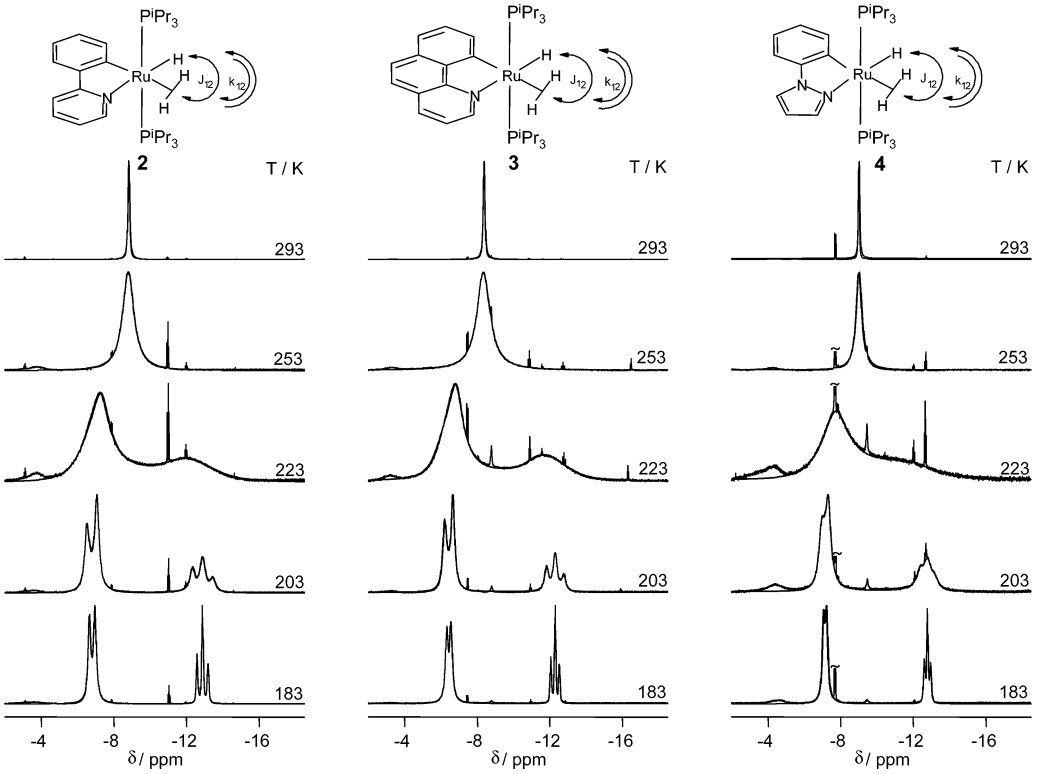

Figure 2. Superimposed experimental and calculated ^{1}H NMR (500 MHz) spectra of the hydride region of **2**−**4** at selected temperatures.

The dependence on temperature of the parameters of the rotational coherent and incoherent exchange rates in **2**−**4** can be expressed by the Arrhenius type equation

$$k = A \exp(-E_a/RT)$$

where k is the corresponding exchange rate, either the incoherent chemical exchange rate k_{12} or the coherent quantum-mechanical exchange rate πJ_{12}. A is the frequency factor, E_a is the activation energy of the observed process, R is the ideal gas constant (8.31 J/(mol·K)), and T is the temperature.

For compound **2** $\pi J_{12} = 10^{5.6\pm0.4} \exp((-10.1 \pm 1.0 \text{ kJ mol}^{-1})/RT)$ Hz (173 K $\le T \le$ 213 K; $J_{12} = 380$ Hz at 213 K) and $k_{12} = 10^{12.7 \pm 0.1} \exp((-40.0 \pm 1.2 \text{ kJ mol}^{-1})/RT)$ s^{-1} (183 K $\le T \le$ 263 K; $k_{12} = 680$ s^{-1} at 213 K).

For compound **3** $\pi J_{12} = 10^{5.6\pm0.3} \exp((-10.7 \pm 1.3 \text{ kJ mol}^{-1})/RT)$ Hz (173 K $\le T \le$ 213 K; $J_{12} = 320$ Hz at 213 K) and $k_{12} = 10^{13.1\pm0.2} \exp((-42.3 \pm 0.8 \text{ kJ mol}^{-1})/RT)$ s^{-1} (183 K $\le T \le$ 263 K; $k_{12} = 540$ s^{-1} at 213 K).

For compound **4** $\pi J_{12} = 10^{6.4\pm0.3} \exp((-13.8 \pm 1.0 \text{ kJ mol}^{-1})/RT)$ Hz (173 K $\le T \le$ 213 K; $J_{12} = 310$ Hz at 213 K) and $k_{12} = 10^{13.3\pm0.1} \exp((-42.0 \pm 0.8 \text{ kJ mol}^{-1})/RT)$ s^{-1} (183 K $\le T \le$ 263 K; $k_{12} = 1050$ s^{-1} at 213 K).

The Arrhenius diagrams of the coherent and incoherent exchanges of the three complexes are plotted in the same graph in Figure 3.

Complexes **1**−**4** are the first known examples of complexes in which both the incoherent (classical) and the coherent (quantum-mechanical) exchange between a hydride and a dihydrogen ligand can be observed experimentally. The exchange in these compounds can be described by simple Arrhenius equations. As expected, the activation energy of the coherent exchange is much smaller than that of the classical chemical exchange. The activation energies of the classical exchange process in the three complexes is hardly dependent upon the complex and is found near 40 kJ mol^{-1}, whereas the activation energies of the coherent process are in the range of 10 kJ mol^{-1}.

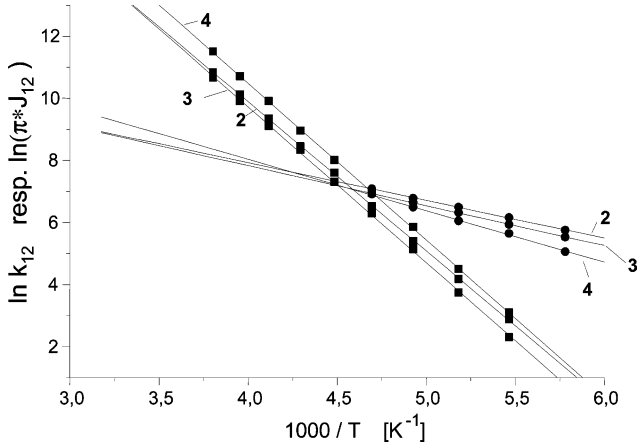

Figure 3. Arrhenius plots of the coherent (●) and incoherent (■) exchange between the hydride and the dihydrogen ligand in **2**−**4**.

We have calculated by DFT at the B3PW91 level the transition states (TS) for the classical exchange process between H and H_2. $\mathbf{2q^{TSQEC}}$−$\mathbf{4q^{TSQEC}}$, respectively, have been located, and they can be described as molecular dihydrogen complexes with the H_2 ligand trans to N and perpendicular to the plane of the chelating ligand (Figure 4 for $\mathbf{2q^{TSQEC}}$). The transition states are not associated with rotation of the H_2 ligand trans to N but connect to the isomer with the dihydrogen trans to C (**2q**−**4q**, respectively) through coupled rotation of H_2 and proton transfer from H_2 to H. This exchange process is sufficient to achieve permutation of two identical particles between H and H_2, which is a necessary

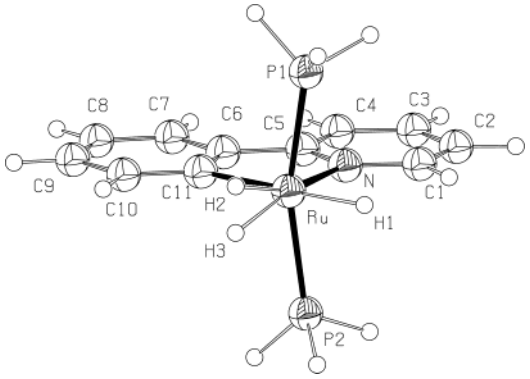

Figure 4. Calculated geometry for the transition state **2q**^{TSQEC}, corresponding to the hydrogen scrambling between H and H_2 in **2q**. See Table 2 for selected bond lengths and angles.

condition to observe quantum exchange couplings.[10] The geometry around the transition-metal center is not greatly modified during the exchange (Table 2). The main changes are an increase of the Ru−C bond distance and a shortening of the Ru−N distance to respond to the change in nature of the corresponding trans ligands (H_2 → H for C and H → H_2 for N).

The calculated activation barriers, $\Delta E^{\ddagger}$, overestimate the corresponding experimental values, E_a, by 10 kJ mol^{-1} (Table 2). However, the three calculated values are very close, as is the case for the experimental data. The discrepancy between calculated and experimental barriers could originate from the highly unfavorable C−Ru−H linear geometry in the transition state, where two strong σ-electron donor groups are mutually trans. In the real systems, C−H···H−Ru interactions between the hydride and dangling bonds within the phosphine ligands may develop and stabilize the TS with respect to the ground state.[11]

The very unusual observation of quantum exchange coupling between hydride and dihydrogen is due to the small reorganization of the molecular geometry during the exchange process (Table 2). This can be traced not only to the chelate nature of the ligands used but also to the nonexistence of the dihydrogen complex isomer with H_2 cis to C as an intermediate along the exchange pathway (shorter tunneling path). Of importance also is the destabilizing nature of the C−Ru−H linear bonding pattern in the TS, leading to an activation barrier for H scrambling of 40 kJ mol^{-1}. This is sufficiently high both to be observed by NMR and to delay the onset of incoherent exchange, so as to have observable coherent exchange.

Reactivity Studies: Dihydrogen Substitution. The dihydrogen ligand in **2** can easily be substituted to give the new complexes RuH(L)(ph-py)(P^iPr_3)$_2$ (L = N_2 (**5**), O_2 (**6**), CO (**7**), C_2H_4 (**8**)), simply by bubbling the corresponding gas into a pentane solution of **2** (Scheme 1). Complexes **5**−**8** were fully characterized by microanalysis and spectroscopic methods (see the Experimental Section). In addition, **6** and **8** were characterized by X-ray analysis (Tables 1 and 3). It should be noted that solutions of **8** are only stable under an atmosphere of ethylene. All complexes display the same structure

Scheme 1. Substitution of the Dihydrogen Ligand in RuH(H_2)(ph-py)(P^iPr_3)$_2$ (2) by N_2 (5), O_2 (6), CO (7), and C_2H_4 (8)

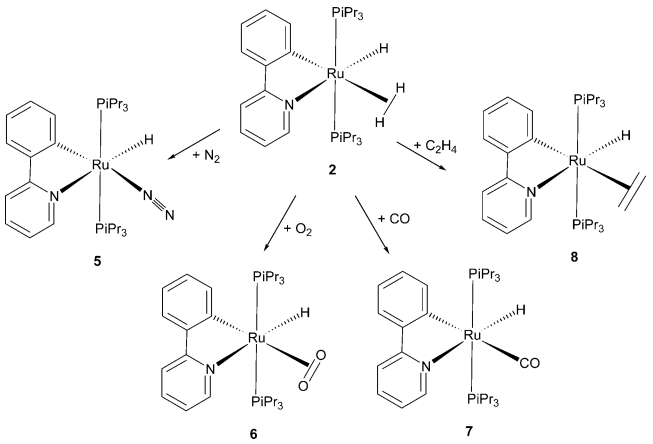

Table 3. Comparison of the Experimental and Calculated Values of Selected Bond Distances (Å) and Angles (deg) for the Dioxygen (6 and 6q) and Ethylene (8 and 8q) Complexes

	6	6q	8	8q
Ru−C	2.084(3)	2.069	2.0895(14)	2.075
Ru−N	2.140(3)	2.141	2.2169(12)	2.210
Ru−P	2.3832(10)	2.319	2.3847(4)	2.294
	2.3905(10)		2.3724(4)	
Ru−H	1.63(3)	1.582	1.47(2)	1.593
C−C			1.395(2)	1.402
O−O	1.407(3)	1.378		
P−Ru−P	162.49(3)	169.9	161.585(14)	160.0
N−Ru−C	76.77(11)	77.2	76.80(5)	77.2

with the hydride trans to the nitrogen of the phenylpyridyl group and cis to L. The most salient spectroscopic features are the hydride signal in ^{1}H NMR and the metalated carbon in ^{13}C NMR, the chemical shifts depending upon the nature of L. Thus, the hydride is found at −12.04 ppm (J_{P-H} = 25.3 Hz) for **5**, −3.10 ppm (J_{P-H} = 19.6 Hz) for **6**, −12.87 ppm (J_{P-H} = 24.7 Hz) for **7**, and −10.87 ppm (J_{P-H} = 24.8 Hz) for **8**. The values are very similar, except for the O_2 complex; precedents for low-field shifts of the hydride upon O_2 coordination are known.[12] The metalated carbons are coupled to phosphorus and resonate at 191.1 ppm (J_{P-C} = 13 Hz) for **5**, 193.4 ppm (J_{P-C} = 9 Hz) for **6**, 191.4 ppm (J_{P-C} = 13 Hz) for **7**, and 199.3 ppm (J_{P-C} = 12 Hz) for **8**. In the case of **8**, we could observe a fluxional behavior which involves both the phosphine and the ethylene ligands. Ethylene was characterized at room temperature by a broad singlet at 2.51 ppm in the ^{1}H NMR spectrum and at 47.0 ppm in the ^{13}C NMR spectrum. The ^{1}H NMR signal shifts to 2.42 ppm at 215 K and decoalesces at lower temperatures into two signals at 2.52 and 2.28 ppm. The activation energy of the rotation process was calculated to be 45.9 kJ mol^{-1}, which is in the range found for other ethylene complexes.[13]

The structural data found for **6** and **8** are very similar to those found for **2** (see Figures 5 and 6). Each complex adopts a slightly distorted octahedral geometry (P−Ru−P angle near 162° in each case), the hydride being

(11) Richardson, T. B.; Koetzle, T. F.; Crabtree, R. H. *Inorg. Chim. Acta* **1996**, *250*, 69.

(12) (a) Jimenez-Tenorio, M.; Puerta, M. C.; Valerga, P. *J. Am. Chem. Soc.* **1993**, *115*, 9794. (b) Jimenez-Tenorio, M.; Puerta, M. C.; Valerga, P. *Inorg. Chem.* **1994**, *33*, 3515.

(13) Cramer, R.; Kline, J. B.; Roberts, J. D. *J. Am. Chem. Soc.* **1969**, *91*, 2519.

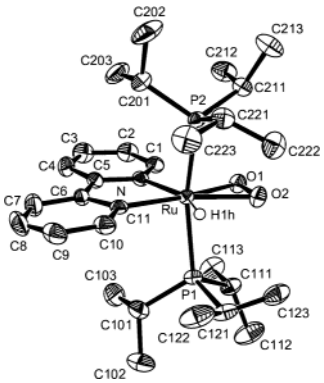

Figure 5. X-ray crystal structure of $RuH(O_2)$(ph-py)($P^iPr_3)_2$ (**6**).

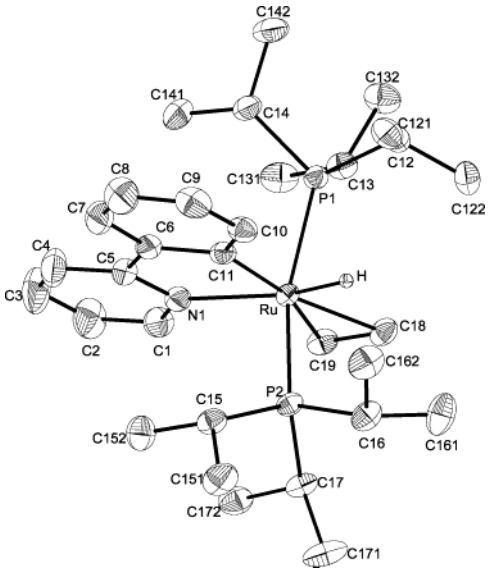

Figure 6. X-ray crystal structure of $RuH(C_2H_4)$(ph-py)($P^iPr_3)_2$ (**8**).

trans to nitrogen. The Ru−C and Ru−N distances for the metalated phenylpyridyl ligands seem little affected by the trans ligand; they are respectively 2.135(3) Å (average values due to disorder) for **2**, 2.084(3) and 2.140(3) Å for **6** and 2.0895(14) and 2.2169(12) Å for **8**. In the case of **6**, the O−O distance is 1.407(3) Å, significantly longer than in free dioxygen (1.2074 Å) but similar to that in other dioxygen ruthenium complexes.[12,1414] Remarkably, the hydride and the dioxygen ligand adopt a cis configuration, as previously reported in the rhodium complex $RhH(O_2)\{CH_2{=}C(CH_2CH_2P^tBu_2)_2\}$.[15] Finally the C−C distance in the ethylene ligand of **8** is also elongated (1.395(2) Å) compared to uncoordinated ethylene (1.33 Å).

The model systems $RuH(L)$(ph-py)$(PH_3)_2$ (L = N_2 (**5q**), O_2 (**6q**), CO (**7q**), C_2H_4 (**8q**)) have been optimized at the DFT level (B3PW91), and for **6q** and **8q** the agreement with the experimental data is excellent (Table 3). The geometry of the 16-electron fragment RuH(ph-py)$(PH_3)_2$ (**A**), with no ligand trans to C, has been optimized. The structure of **A** is that of an octahedron lacking one ligand trans to C. The binding energies, ΔE_b, to **A** of the various ligands range from 88.3 kJ mol^{-1} (H_2, **2q**) to 215.6 kJ mol^{-1} (CO, **7q**), and the dihydrogen complex is the least stable (Table 4). The substitution of H_2 by the L ligand is thus thermodynamically favored for all the ligands considered. The Ru−C bond distance trans to the incoming ligand L tends to slightly increase with the binding energy ΔE_b, in agreement with the presence of stronger σ-donor ligands (Table 4). The other bonds around the metal center are not altered in a similar fashion. The Ru−H and Ru−N bond distances are not correlated with each other. **8q** exhibits both a long Ru−H bond (1.647 Å) and a long Ru−N bond (2.210 Å), while the opposite is observed for **6q** (short Ru−H, 1.582 Å; short Ru−N, 2.141 Å).

Table 4. Selected Bond Distances (Å) for the Complexes $RuH(L)$(ph-py)$(PH_3)_2$ (L = H_2 (2q), N_2 (5q), O_2 (6q), CO (7q), C_2H_4 (8q)) and ΔE_b Bonding Energies (kcal mol^{-1}) of the Different L Ligands to the Fragment RuH(ph-py)$(PH_3)_2$

	2q	5q	6q	7q	8q
Ru−C	2.063	2.060	2.069	2.110	2.075
Ru−N	2.174	2.174	2.141	2.179	2.210
Ru−H	1.610	1.611	1.582	1.606	1.647
ΔE_b	88.3	98.5	103.4	215.6	116.4

The dihydrogen ligand can be eliminated by refluxing **2** in THF to form the new species **9**. This complex can also be formed by slow loss of ethylene from **8** in a THF solution. **9** is very air-sensitive and immediately reacts with H_2, N_2, O_2, CO, or C_2H_4 to give the corresponding complexes **2** and **5**−**8**. It has not been possible to isolate it, and therefore, **9** has only been characterized in solution. Complex **9** is not fluxional; it shows a hydride signal at −10.95 ppm (J_{P-H} = 26.4 Hz) and a metalated carbon at 185.0 ppm (J_{P-C} = 11.6 Hz). **9** may be a 16-electron species or a complex resulting from the substitution of H_2 or C_2H_4 by THF. In view of the similarity of the spectroscopic properties of **9** with those of **2** and **5**−**8** and of its absence of fluxionality, we propose for **9** the 18-electron structure $RuH(THF)$(ph-py)($P^iPr_3)_2$.

This series of experiments demonstrates (i) that the exchange process in the hydrido dihydrogen derivatives is not highly dependent upon the structure of the metalated ligand and, in particular, it is not affected by the rigidity of the benzoquinoline ligand and (ii) that the dihydrogen ligand is readily substituted by many different ligands. Of special interest are the dioxygen complex, one of the few cis hydrido dioxygen compounds known, and the ethylene complex. In the latter compound, no evidence has been found for the insertion of ethylene either into the Ru−H or into the Ru−C bond. This contrasts with what is observed in the corresponding complexes $RuH(H_2)(O{=}C(R)C_6H_4)(PR_3)_2$, which have been shown to catalyze the insertion of ethylene into the C−H bond of an aromatic ketone at room temperature.[4]

To gain a better understanding of the absence of reaction of the ethylene complex **8**, we have searched for a possible reaction mechanism. The ethylene complex **8q′** with the ethylene ligand cis to C has been optimized, and it is less stable than **8q** by only 26 kJ mol^{-1}. This intermediate is on the pathway for the C−C bond coupling process, and its energy relative to **8q** is not high enough to explain the absence of reaction. However, the isomerization of **8q** to **8q′** would most

(14) Jia, G.; Sang Ng, W.; Chu, H. S.; Wong, W.-T.; Yu, N.-T.; Williams, I. D. *Organometallics* **1999**, *18*, 3597 and references therein.
(15) Vigalok, A.; Shimon, L. J. W.; Milstein, D. *J. Chem. Soc., Chem. Commun.* **1996**, 1673.

Scheme 2. Isomerization of the Ethylene Complexes 8q and 8q′

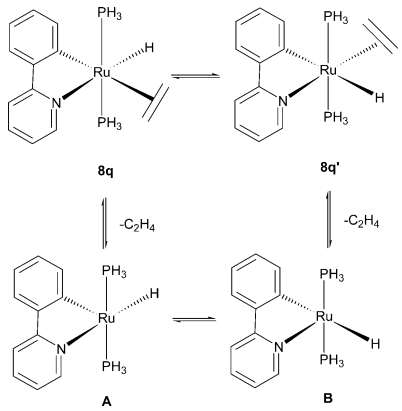

likely occur first through dissociation of C_2H_4, which requires 116.4 kJ mol^{-1}. The 16-electron complex **A** with the hydride trans to N has then to isomerize to the 16-electron complex **B** with the hydride cis to N (Scheme 2). The reaction energy associated to the **A** → **B** isomerization is +77.3 kJ mol^{-1} with an activation energy of 80.1 kJ mol^{-1}. The strong endothermicity of the transformation **A** → **B** is a consequence of the unfavorable linear C−Ru−H geometry in **B**, where two strong σ-electron donor groups are mutually trans. Thus, the activation energy for the transformation **8q** → **8q′** amounts to 196.5 kJ mol^{-1}, which is the sum of the dissociation energy of C_2H_4 from **8q** and the activation energy for the isomerization of the 16-electron complex **A**. The transition state **8q′^{TS}** for ethylene insertion into the Ru−H bond from **8q′** has been located and lies 54.5 kJ mol^{-1} above **8q′**. Although the insertion mechanism is not too high in energy, the rate-determining step is the isomerization of **8q** to **8q′** and this process is too endothermic. We have tried to locate a transition state for ethylene insertion into Ru−H from **8q** leading to an ethyl complex, but all our attempts have failed. The trans configuration of the two Ru−C bonds in the TS would be highly destabilizing. All these observations tend to indicate that, in the catalytic cycle for the Murai reaction, the interplay of the nature of the mutually trans ligands plays a critical role. In Murai's system, the ketone group in acetophenone is certainly essential to induce selective ortho metalation of the phenyl ring.[3] However, the reaction can only proceed, and particularly achieve C−C coupling, through a low-energy pathway displaying an intermediate complex with ethylene cis to the ortho-metalated carbon. One possibility could be decoordination of the ketone group, hence creating a vacant site cis to the aryl group. The dissociation of the orienting group is certainly easier for a ketone than for pyridine. Strong coordination of pyridine might explain the absence of reaction in the phenylpyridine case.

Summary

We have reported in this paper the synthesis of new hydrido dihydrogen complexes containing an ortho-metalated ligand (phenylpyridine, benzoquinoline, or phenylpyrazole). These complexes display remarkable spectroscopic properties: namely, they show exchange couplings between the hydride and the dihydrogen ligands. The origin of these couplings lies in the barrier necessary to exchange the hydride with one of the dihydrogen protons. The dihydrogen ligand in these complexes may readily be substituted by dinitrogen, dioxygen, carbon monoxide, or ethylene. Remarkably, ethylene does not insert either into the Ru−H or into the Ru−C bond. The computational studies have allowed us not only to ascertain the location of the hydride and dihydrogen ligands in the different complexes but also to fully understand the mechanism of the exchange process and to highlight the importance of the chelating assistance in the catalytic cycle for the Murai reaction and of the interplay of the mutually trans ligands.

Experimental Section

All reactions were carried out under argon by using Schlenk glassware and vacuum-line or glovebox techniques. All solvents were freshly distilled from standard drying agents and thoroughly degassed under argon before use. Microanalyses were performed by the Laboratoire de Chimie de Coordination Microanalytical Service. ^{1}H (200.13, 250.13, 300.13, or 500.13 MHz), ^{13}C (125.70 MHz), and ^{31}P NMR spectra (201.46 MHz) were recorded on Bruker or Varian instruments operating in the Fourier transform mode. Tetrahydrofuran-$^2H_8$ used for NMR analysis was distilled before use and thoroughly degassed during four freezing, thawing, and degassing cycles. All NMR samples were prepared in either flame-sealed (ca. 10^{-6} mbar) or Teflon-stoppered NMR tubes. $RuCl_3 \cdot 3H_2O$ was purchased from Johnson Matthey Ltd. $RuH_2(H_2)_2(PCy_3)_2$ was prepared according to the procedure described in ref 6b.

$RuH(H_2)(ph\text{-}py)(PCy_3)_2$ (1). To a suspension of $RuH_2(H_2)_2(PCy_3)_2$ (265 mg, 0.40 mmol) in 20 mL of pentane was added 2-phenylpyridine (74 μL, 0.52 mmol) at room temperature. The reaction was allowed to proceed for 24 h, during which time an orange solid precipitated. This orange precipitate was filtered off, washed with 20 mL of pentane, and dried in vacuo. Yield: ca. 86%. Anal. Calcd for $RuC_{47}H_{77}P_2N$: C, 68.91; H, 9.47; N, 1.71. Found: C, 68.23; H, 9.54; N, 1.67. ^{1}H NMR (400.13 MHz, C_6D_6, 296 K; δ): −8.44 (br, 3H, Ru*H*(H_2)); 1.11−2.33 (m, 66H, P*Cy*$_3$); 6.57 (t, 1H, $^1J_{HH}$ = 6.0 Hz), 7.19 (t, 1H, $^1J_{HH}$ = 8.6 Hz), 7.21 (t, 1H, $^1J_{HH}$ = 7.6 Hz), 7.35 (m, 1H), 7.75 (d, 1H, $^1J_{HH}$ = 8.4 Hz), 7.91 (d, 1H, $^1J_{HH}$ = 7.4 Hz), 8.61 (d, 1H, $^1J_{HH}$ = 7.4 Hz) (all for ph-py); 9.62 (d, 1H, $^1J_{HH}$ = 5.9 Hz, *H1*). ^{31}P{^{1}H} NMR (81. 01 MHz, C_6D_6, 296 K; δ, ppm): 46.4 (s). T_1 (400.13 MHz, THF-d_8): 293 K, $\delta_{-8.8}$ 25 ms; 170 K, $\delta_{-6.9}$ 873 ms, $\delta_{-13.0}$ 1061 ms; 183 K, $\delta_{-6.9}$ 105 ms, $\delta_{-12.9}$ 267 ms.

$RuH(H_2)(ph\text{-}py)(P^iPr_3)_2$ (2). A solution of Ru(COD)(COT) (**1**; 80 mg, 0.25 mmol) with 2 equiv of commercially available triisopropylphosphine (97 μL, 0.50 mmol) and 1 equiv of 2-phenylpyridine (36 μL, 0.25 mmol) was filtered into a Fisher−Porter bottle and afterward pressurized with 3 bar of H_2 over 24 h at room temperature. The solvent was eliminated under vacuum, and the resulting red oil was dried for 12 h with a high-vacuum pump. Then 10 mL of pentane was added, whereby a red solid precipitated. After filtration the filtrate was kept in the freezer at −20 °C for 12 h. The resulting red crystals were collected. Yield: ca. 86%. Anal. Calcd for $RuC_{29}H_{53}P_2N$: C, 60.18; H, 9.23; N, 2.42. Found: C, 59.83; H, 8.81; N, 2.43. ^{1}H NMR (500.13

MHz, THF-d_8, 293 K; δ): −8.82 (br, 3H, Ru*H*(H_2)), 0.84 (m, 18H, P(CH*Me*$_2$)$_3$), 1.01 (m, 18H, P(CH*Me*$_2$)$_3$), 1.78 (m, 6H, P(C*H*Me$_2$)$_3$), 6.71 (t, 1H, $^1J_{HH}$ = 7.2 Hz, *H8*), 6.74 (t, 1H, $^1J_{HH}$ = 7.2 Hz, *H9*), 6.82 (t, 1H, $^1J_{HH}$ = 6.4 Hz, *H2*), 7.53 (t, 1H, $^1J_{HH}$ = 7.6 Hz, *H3*), 7.66 (d, 1H, $^1J_{HH}$ = 7.6 Hz, *H7*), 7.87 (d, 1H, $^1J_{HH}$ = 8.1 Hz, *H4*), 8.04 (d, 1H, $^1J_{HH}$ = 6.9 Hz, *H10*), 9.42 (d, 1H, $^1J_{HH}$ = 5.3 Hz, *H1*). ^{31}P{^{1}H} NMR (201.46 MHz, THF-d_8, 293 K; δ): 57.61(s). ^{13}C{^{1}H} NMR (125.70 MHz, THF-d_8, 293 K; δ): 20.0 (s, P(CH*Me*$_2$)$_3$), 20.4 (s, P(CH*Me*$_2$)$_3$), 27.2 (t, J_{PC} 8.9 Hz, P(C*H*Me$_2$)$_3$), 119.0 (s, *C4*), 119.4 (s, *C8*), 120.0 (s, *C2*), 124.1 (s, *C7*), 127.0 (s, *C9*), 134.3 (s, *C3*), 145.1 (s, *C10*), 145.8 (s, *C6*), 158.0 (s, *C1*), 167.0 (s, *C5*), 197.3 (t, J_{PC} = 10.9 Hz, *C11*).

RuH(H_2)(bq)(P^{i}Pr$_3$)$_2$ (3). A yellow pentane solution (ca. 15 mL) of Ru(COD)(COT) (0.70 g, 2.22 mmol), 7,8-benzoquinoline (0.40 g, 2.22 mmol), and P^{i}Pr$_3$ (0.85 mL, 4.44 mmol) was filtered into a Fischer−Porter bottle and pressurized, at room temperature, with dihydrogen (3 bar). The solution immediately became orange and then, after stirring for a further 24 h, deep red. After attainment of atmospheric pressure, decantation, and then filtration into another Fisher−Porter bottle, the solution was freeze−thawed and degassed. Concentration in vacuo and refrigeration gave a sample of **3** suitable for single-crystal X-ray diffraction analysis. Subsequent concentration of the solvent and storage at room temperature gave **3** as large red cubes. Removal of the mother liquor by decantation and refrigeration gave an additional crop of **3** as a microcrystalline solid. Total yield: 1.2 g, 90%. Anal. Calcd for $RuC_{31}H_{53}P_2N$: C, 61.79; H, 8.80; N, 2.33. Found: C, 61.78; H, 9.07; N, 2.44. ^{1}H NMR (500.13 MHz, THF-d_8, 293 K; δ): −8.55 (br, 3H, RuH_3), 0.69 (m, 18H, P(CH*Me*$_2$)$_3$), 0.95 (m, 18H, P(CH*Me*$_2$)$_3$), 1.70 (m, 6H, P(C*H*Me$_2$)$_3$), 7.21 (m, 1H, *H9*), 7.26 (m, 2H, *H2*/*H8*), 7.47 (d, 1H, $^1J_{HH}$ = 8.6 Hz, *H5*), 7.66 (d, 1H, $^1J_{HH}$ = 8.6 Hz, *H6*), 8.06 (d, 1H, $^1J_{HH}$ = 7.7 Hz, *H3*), 8.28 (d, 1H, $^1J_{HH}$ = 6.7 Hz, *H10*), 9.73 (d, 1H, $^1J_{HH}$ = 4.8 Hz, *H1*). ^{31}P{^{1}H} NMR (201.46 MHz, THF-d_8, 298 K; δ): 57.65 (s). ^{13}C{^{1}H} NMR (125.70 MHz, THF-d_8, 298 K; δ): 19.8 (s, P(CH*Me*$_2$)$_3$), 20.3 (s, P(CH*Me*$_2$)$_3$), 27.3 (t, J_{PC} = 8.8 Hz, P(C*H*Me$_2$)$_3$), 118.0 (s, *C8*), 120.1 (s, *C2*), 123.1 (s, *C5*), 127.22 (s, *C9*), 127.59 (s, *C4*), 130.83 (s, *C6*), 133.22 (s, *C3*), 134.8 (s, *C7*), 142.1 (s, *C10*) 142.8 (s, *C12*), 155.8 (s, *C1*), 157.1 (s, *C13*), 195.0 (t, J_{PC} 11.1 Hz, *C11*). T_1 (500.13 MHz, THF-d_8): 273 K, $\delta_{-8.5}$ 40.16 ms; 183 K, $\delta_{-6.6}$ (d, 2H, J_{HH} = 121 Hz) 40 ms, $\delta_{-12.6}$ (tt, 1H, J_{HH} = 121 Hz, J_{HP} = 21.4 Hz) 79 ms; 173 K, $\delta_{-6.6}$ (d, 2H, J_{HH} = 85 Hz) 51 ms, $\delta_{-12.6}$ (tt, 1H, J_{HH} = 85 Hz, J_{HP} = 21.7 Hz) 178 ms.

RuH(H_2)(ph-pz)(P^{i}Pr$_3$)$_2$ (4). A yellow pentane solution (ca. 10 mL) of Ru(COD)(COT) (0.70 g, 2.22 mmol), 1-phenylpyrazole (0.29 mL, 2.22 mmol), and P^{i}Pr$_3$ (0.85 mL, 4.44 mmol) was filtered into a Fisher−Porter bottle and pressurized, at room temperature, with dihydrogen (3 bar). The mixture immediately became very pale yellow. After it was stirred at room temperature for 24 h, the solution was worked up in a manner similar to that described for **3** to yield an orange solution. Storage at −20 °C overnight gave **4** as a pale yellow microcrystalline solid. Total yield: 1.0 g, 80%. Anal. Calcd for $RuC_{27}H_{53}P_2N_2$: C, 57.04; H, 9.33; N, 4.93. Found (1): C, 59.88; H, 8.61; N, 6.02. Found (2): C, 59.31; H, 8.59; N, 5.89. ^{1}H NMR (500.13 MHz, THF-d_8, 293 K; δ): −9.22 (br, 3H, RuH_3), 0.82 (m, 18H, P(CH*Me*$_2$)$_3$), 1.04 (m, 18H, P(CH*Me*$_2$)$_3$), 1.70 (m, ∼6H, P(C*H*Me$_2$)$_3$, under solvent peak); 6.41 (t, 1H, $^1J_{HH}$ = 2.05 Hz, *H2*), 6.68 (m, 2H, *H6*/*H7*), 7.20 (dd, 1H, $^1J_{HH}$ = 7.34 Hz, 1.2 Hz, *H5*), 7.92 (d, 1H, $^1J_{HH}$ = 6.75 Hz, *H8*), 7.96 (b, 1H, *H3*), 8.28 (d, 1H, $^1J_{HH}$ = 1,8 Hz, *H1*). ^{31}P{^{1}H} NMR (201.46 MHz, THF-d_8, 298 K; δ): 57.65 (s). ^{13}C{^{1}H} NMR (125.70 MHz, THF-d_8, 298 K; δ): 19.79 (s, P(CH*Me*$_2$)$_3$), 20.21 (s, P(CH*Me*$_2$)$_3$), 27.14 (t, J_{PC} = 8.8 Hz, P(C*H*Me$_2$)$_3$), 108.1 (s, *C2*), 111.6 (s, *C6*), 119.3 (s, *C5*), 120.13 (s, *C7*), 124.53 (s, *C1*), 124.57 (s, *C8*), 130.0 (s, *C4*), 144.18 (s, *C3*), 145.92 (s, *C9*), 176.37 (t, J_{PC} = 11.3 Hz, *C9*). T_1 (500.13 MHz, THF-d_8): 273 K, $\delta_{-9.2}$ 51 ms; 183 K, $\delta_{-7.3}$ (d, 2H, J_{HH} = 86 Hz) 42 ms, $\delta_{-13.1}$ (tt, 1H, J_{HH} = 86 Hz, J_{HP} = 19.4 Hz) 82 ms; 173 K, $\delta_{-7.3}$ (s, 2H) 56 ms, $\delta_{-13.1}$ (tt, 1H, J_{HH} = 54 Hz, J_{HP} = 21.7 Hz) 160 ms.

RuH(N_2)(ph-py)(P^{i}Pr$_3$)$_2$ (5). N_2 was bubbled through a pentane solution (20 mL) of RuH(H_2)[P(^{i}Pr)$_3$]$_2$(phpy) (**2**; 150 mg, 0.25 mmol) until all pentane was evaporated (10 min). The resulting green powder was dried in vacuo. Yield: ca. 90%. Anal. Calcd for $RuC_{29}H_{51}P_2N_3$: C, 57.60; H, 8.50; N, 6.95. Found: C, 57.74; H, 8.22; N, 6.26. ^{1}H NMR (500.13 MHz, THF-d_8, 293 K; δ): −12.04 (t, J_{PH} = 25.3 Hz, 1H, RuH), 0.83 (m, 18H, P(CH*Me*$_2$)$_3$), 1.16 (m, 18H, P(CH*Me*$_2$)$_3$), 2.06 (m, 6H, P(C*H*Me$_2$)$_3$), 6.69 (t, 1H, $^1J_{HH}$ = 6.8 Hz, *H8*), 6.72 (dt, 1H, $^1J_{HH}$ = 7.2 Hz, $^2J_{HH}$ = 1.9 Hz, *H9*), 7.04 (t, 1H, $^1J_{HH}$ = 6.4 Hz, *H2*), 7.59 (m, 2H, *H3* and *H7*), 7.65 (d, 1H, $^1J_{HH}$ = 6.8 Hz, *H4*), 7.88 (d, 1H, $^1J_{HH}$ = 8.1 Hz, *H10*), 9.24 (d, 1H, $^1J_{HH}$ = 5.6 Hz, *H1*). ^{31}P{^{1}H} NMR (201.46 MHz, THF-d_8, 293 K; δ): 48.69 ppm. ^{13}C{^{1}H} NMR (125.70 MHz, THF-d_8, 293 K; δ): 19.4 (s, P(CH*Me*$_2$)$_3$), 19.9 (s, CH*Me*$_2$)$_3$), 26.4 (t, J_{PC} = 8.6 Hz, P(C*H*Me$_2$)$_3$), 119.1 (s, *C4*), 119.9 (s, *C8*), 120.2 (s, *C2*), 123.5 (s, *C7*), 127.2 (s, *C9*), 134.2 (s, *C3*), 143.8 (s, *C10*), 146.2 (s, *C6*), 152.0 (s, *C1*), 167.2 (s, *C5*), 191.1 (t, J_{PC} = 13.4 Hz, *C11*).

RuH(O_2)(ph-py)(P^{i}Pr$_3$)$_2$ (6). O_2 was bubbled through a pentane solution (20 mL) of **2** (150 mg, 0.25 mmol) for 5 min. The solution was kept at −20 °C for 24 h, allowing the formation of hexagonal orange crystals. Yield: ca. 90%. Anal. Calcd for $RuC_{29}H_{51}P_2NO_2$: C, 57.22; H, 8.44; N, 2.30. Found: C, 57.40; H, 8.58; N, 2.33. ^{1}H NMR (500.13 MHz, THF-d_8, 293 K; δ): −3.10 (t, 1H, $^2J_{PH}$ = 19.6 Hz, RuH), 0.80 (m, 18H, P(CH*Me*$_2$)$_3$), 1.05 (m, 18H, P(CH*Me*$_2$)$_3$), 1.87 (m, 6H, P(C*H*Me$_2$)$_3$), 6.81 (t, 1H, $^1J_{HH}$ = 7.4 Hz, *H8*), 6.86 (t, 1H, $^1J_{HH}$ = 7.2 Hz, *H9*), 7.18 (t, 1H, $^1J_{HH}$ = 6.5 Hz, *H2*), 7.71 (t, 1H, $^1J_{HH}$ = 7.6 Hz, *H3*), 7.78 (d, 1H, $^1J_{HH}$ = 7.4 Hz, *H7*), 7.97 (d, 1H, $^1J_{HH}$ = 8.1 Hz, *H4*), 8.38 (d, 1H, $^1J_{HH}$ = 7.4 Hz, *H10*), 10.22 (d, 1H, $^1J_{HH}$ = 5.1 Hz, *H1*). ^{31}P{^{1}H} NMR (201.46 MHz, THF-d_8, 293 K; δ): 32.72. ^{13}C{^{1}H} NMR (125.70 MHz, THF-d_8, 293 K; δ): 19.5 (s, P(CH*Me*$_2$)$_3$), 20.2 (s, P(CH*Me*$_2$)$_3$), 24.0 (t, J_{PC} = 8.6 Hz, P(C*H*Me$_2$)$_3$), 119.2 (s, *C4*), 120.2 (s, *C8*), 121.0 (s, *C2*), 124.8 (s, *C7*), 128.0 (s, *C9*), 136.2 (s, *C3*), 143.1 (s, *C10*), 146.5 (s, *C6*), 154.5 (s, *C1*), 165.5 (s, *C5*), 193.4 (t, J_{PC} = 9.2 Hz, *C11*).

RuH(CO)(ph-py)(P^{i}Pr$_3$)$_2$ (7). Carbon monoxide was bubbled into a pentane solution (20 mL) of **2** (364 mg, 0.63 mmol) for 5 min. The solvent was eliminated under vacuum, and the resulting yellow powder was dried in vacuo. Anal. Calcd for $RuC_{30}H_{51}P_2ON$: C, 59.77; H, 8.68; N, 2.29. Found: C, 59.58; H, 8.50; N, 2.32. IR (cm^{-1}, Nujol): 1891 (Ru−CO). ^{1}H NMR (500.13 MHz, THF-d_8,

293 K; δ): −12.87 (t, J_{PH} = 24.7 Hz, 1H, RuH), 0.83 (m, 18H, P(CH*Me*$_2$)$_3$), 1.15 (m, 18H, P(CH*Me*$_2$)$_3$), 2.06 (m, 6H, P(C*H*Me$_2$)$_3$), 6.81 (m, 2H, *H8*/*H9*), 6.96 (t, 1H, $^1J_{HH}$ = 6.3 Hz, *H2*), 7.60 (t, 1H, $^1J_{HH}$ = 7.6 Hz, *H3*), 7.68 (m, 1H, *H7*), 7.84 (m, 1H, *H4*), 7.88 (d, 1H, $^1J_{HH}$ = 8.2 Hz, *H10*), 9.37 (d, 1H, $^1J_{HH}$ = 5.4 Hz, *H1*). ^{31}P{^{1}H} NMR (201.46 MHz, THF-d_8, 293 K; δ): 51.72 ppm. ^{13}C{^{1}H} NMR (125.70 MHz, THF-d_8, 293 K; δ): 19.6 (s, P(CH*Me*$_2$)$_3$), 20.1 (s, CH*Me*$_2$)$_3$), 27.9 (t, J_{PC} = 9.8 Hz, P(C*H*Me$_2$)$_3$), 119.4 (s, *C4*), 120.5 (s, *C8*), 121.5 (s, *C2*), 123.8 (s, *C7*), 127.3 (s, *C9*), 135.1 (s, *C3*), 144.4 (s, *C10*), 147.2 (s, *C6*), 155.7 (s, *C1*), 167.5 (s, *C5*), 191.4 (t, J_{PC} 13.4 Hz, *C11*), 207.3 (t, J_{PC} = 12.8 Hz, *C*O).

RuH(C$_2$H$_4$)(ph-py)(P^{i}Pr$_3$)$_2$ (8). C_2H_4 was bubbled through a pentane solution (20 mL) of **2** (150 mg, 0.25 mmol) for 5 min. The resulting red solution was filtered and transferred into a Fisher−Porter bottle. It was stored under 3 bar of C_2H_4 at −20 °C overnight. The resulting orange crystals were stored under 3 bar of C_2H_4. A suitable NMR sample can be obtained under 800 mbar of C_2H_4. Yield: ca. 65%. Anal. Calcd for $C_{31}H_{55}NP_2Ru$: C, 61.56; H, 9.17; N, 2.32. Found C, 60.93; H, 8.96; N, 2.16. ^{1}H NMR (500.13 MHz, THF-d_8, 293 K; δ): −10.87 (t, $^2J_{PH}$ = 24.8 Hz, 1H, RuH), 0.74 (m, 18H, P(CH*Me*$_2$)$_3$), 1.05 (m, 18H, P(CH*Me*$_2$)$_3$), 1.63 (m, 6H, P(C*H*Me$_2$)$_3$), 2.51 (br, 4H, η^2-C$_2$H$_4$), 6.70 (m, 2H, *H8*/*H9*), 7.00 (t, 1H, $^1J_{HH}$ = 6.5 Hz, *H2*), 7.57 (t, 1H, $^1J_{HH}$ = 7.6 Hz, *H3*), 7.72 (m, 1H, *H7*), 7.93 (d, 1H, $^1J_{HH}$ = 8.3 Hz, *H4*), 8.34 (d, 1H, $^1J_{HH}$ = 6.9 Hz, *H10*), 9.84 (d, 1H, $^1J_{HH}$ = 5.7 Hz, *H1*); uncoordinated C_2H_4 is observed at 5.35 ppm. ^{31}P{^{1}H} NMR (201.46 MHz, THF-d_8, 293 K; δ): 37.18 ppm. ^{13}C{^{1}H} NMR (125.70 MHz, THF-d_8, 293 K; δ): 20.2 (s, P(CH*Me*$_2$)$_3$), 21.0 (s, CH*Me*$_2$)$_3$), 25.4 (partially hidden by THF signal, P(C*H*Me$_2$)$_3$), 47.0 (s, η^2-C$_2$H$_4$), 118.9 (s, *C4*), 119.4 (s, *C8*), 120.5 (s, *C2*), 124.5 (s, *C7*), 126.4 (s, *C9*), 134.7 (s, *C3*), 145.1 (s, *C6*), 147.0 (s, *C10*), 155.5 (s, *C1*), 169.6 (s, *C5*), 199.3 (t, J_{PC} = 12.0 Hz, *C11*); uncoordinated C_2H_4 is observed at 123.3 ppm.

RuH(THF)(ph-py)(P^{i}Pr$_3$)$_2$ (9). A solution of 300 mg (0.51 mmol) of **2** in THF was heated to reflux for 3 h inside a Schlenk bulb equipped with a Young tap to avoid grease contamination. During the reaction a slight Ar stream was passed over the solution from time to time. The deep red reaction mixture was cooled to room temperature, and the THF was removed in vacuo. The resulting deep red solid was dried at 10^{-6} mbar for 1 h. ^{1}H NMR (500.13 MHz, THF-d_8, 293 K; δ): −10.95 (t, J_{PH} = 26.4 Hz, 1H, RuH), 0.77 (m, 18H, P(CH*Me*$_2$)$_3$), 0.95 (m, 18H, P(CH*Me*$_2$)$_3$), 2.06 (m, 6H, P(C*H*Me$_2$)$_3$), 6.38 (m, 2H, *H6* and *H7*), 6.96 (t, 1H, $^1J_{HH}$ = 6.4 Hz, *H2*), 7.33 (m, 1H, *H4*), 7.37 (m, 1H, *H7*), 7.50 (t, 1H, $^1J_{HH}$ = 7.6 Hz, *H3*), 7.82 (d, 1H, $^1J_{HH}$ = 8.3 Hz, *H10*), 9.28 (d, 1H, $^1J_{HH}$ = 5.6 Hz, *H1*). ^{31}P{^{1}H} NMR (201.46 MHz, THF-d_8, 293 K, δ): 54.05 ppm. ^{13}C{^{1}H} NMR (125.70 MHz, THF-d_8, 293 K; δ): 19.4 (s, P(CH*Me*$_2$)$_3$), 20.0 (s, CH*Me*$_2$)$_3$), 26.2 (t, J_{PC} = 9.8 Hz, P(C*H*Me$_2$)$_3$), 116.0 (s, *C4*), 118.6 (s, *C8*), 119.4 (s, *C2*), 123.3 (s, *C7*), 125.3 (s, *C9*), 132.1 (s, *C3*), 143.6 (s, *C10*), 143.7 (s, *C6*), 152.6 (s, *C1*), 166.0 (s, *C5*), 185.0 (t, J_{PC} = 11.6 Hz, *C11*).

X-ray Analysis. Data were collected at low temperature (T = 150 K for **2**, 113 K for **3**, 180 K for **6**, and 183 K for **8**) on a Stoe imaging plate diffraction system (IPDS) for **2**, **3**, and **6** and on a Bruker XPS diffraction system (CCD Area detector) in the case of **8**, both equipped with an Oxford Cryosystems Cryostream Cooler Device and using graphite-monochromated Mo Kα radiation (λ = 0.710 73 Å). The final unit cell parameters were obtained by least-squares refinement of a set of 8000 well-measured reflections, and crystal decay was monitored by measuring 200 reflections by image. No significant fluctuation of the intensities was observed. An empirical absorption correction was performed using SADABS[16] (for complex **8**). Structures were solved by means of direct methods using the program SIR92[17] and refined by least-squares procedures on F^2 using the program SHELXL-97,[16] included in the WINGX[18] version 1.64 05. The atomic scattering factors were taken from ref 19. All hydrogen atoms were located on a difference Fourier map, but they were introduced in the refinement as fixed contributors using a riding model with an isotropic thermal parameter fixed at 20% higher than those of the C(sp^2) atoms and 50% higher than those for the C(sp^3) atoms to which they were connected; the methyl groups were refined with the torsion angle as a free variable. The hydride atoms of compounds **3**, **6**, and **8** were isotropically refined. All non-hydrogen atoms were anisotropically refined, and weighting schemes were used in the last cycles of refinement. Weights are calculated from the following formula: $w = 1/[\sigma^2(F_o^2) + (aP)^2 + bP]$, where $P = (F_o^2 + 2F_c^2)/3$. Compound **2** crystallizes in an orthorhombic system with the centrosymmetric space group *Pbcn* and is organized around an inversion center. Consequently, the nitrogen and the C(1) atoms are statistically distributed on both sides of the inversion center, giving rise to a pseudo-centrosymmetry. As a result, it was impossible to locate the hydride atoms in **2**. Drawings of the molecules were performed by using the program ORTEP3[20] with 50% probability displacement ellipsoids for non-hydrogen atoms.

Computational Details. All the calculations were performed at the DFT level (B3PW91)[21] with the Gaussian 98 set of programs.[22] Ru and P atoms were represented with relativistic effective core pseudopotentials (RECP) of the Stuttgart group[23] and the associated basis set augmented with a polarization

(16) Sheldrick, G. M. SHELX-97 and SADABS Programs for Crystal Structure Analysis (Release 97-2); University of Göttingen, Göttingen, Germany, 1998.

(17) Altomare, A.; Cascarano, G.; Giacovazzo C.; Guagliardi, A. SIR92-A Program for Crystal Structure Solution. *J. Appl. Crystallogr.* **1993**, *26*, 343.

(18) Farrugia, L. J. WINGX. *J. Appl. Crystallogr.* **1999**, *32*, 837.

(19) *International Tables for X-ray Crystallography*; Kynoch Press: Birmingham, England, 1974; Vol. IV.

(20) Farrugia, L. J. ORTEP3 for Windows. *J. Appl. Crystallogr.* **1997**, *30*, 565.

(21) (a) Becke, A. D. *J. Chem. Phys.* **1993**, *98*, 5648. (b) Perdew, J. P.; Wang, Y. *Phys. Rev. B* **1992**, *82*, 284.

(22) Frisch, M. J.; Trucks, G. W.; Schlegel, H. B.; Scuseria, G. E.; Robb, M. A.; Cheeseman, J. R.; Zakrzewski, V. G.; Montgomery, J. A.; Stratmann, R. E.; Burant, J. C.; Dapprich, S.; Millam, J. M.; Daniels, A. D.; Kudin, K. N.; Strain, M. C.; Farkas, O.; Tomasi, J.; Barone, V.; Cossi, M.; Cammi, R.; Mennucci, B.; Pomelli, C.; Adamo, C.; Clifford, S.; Ochterski, J.; Petersson, G. A.; Ayala, P. Y.; Cui, Q.; Morokuma, K.; Malick, D. K.; Rabuck, A. D.; Raghavachari, K.; Foresman, J. B.; Cioslowski, J.; Ortiz, J. V.; Stefanov, B. B.; Liu, G.; Liashenko, A.; Piskorz, P.; Komaromi, I.; Gomperts, G.; Martin, R. L.; Fox, D. J.; Keith, T.; Al-Laham, M. A.; Peng, C. Y.; Nanayakkara, A.; Gonzalez, C.; Challacombe, M.; Gill, P. M. W., Johnson, B. G.; Chen, W.; Wong, M. W.; Andres, J. L.; Head-Gordon, M.; Replogle, E. S.; Pople, J. A. *Gaussian 98*, Revision A.7; Gaussian Inc., Pittsburgh, PA, 1998.

(23) (a) Andrae, D.; Haüssermann, U.; Dolg, M.; Stoll, H.; Preuss, H. *Theor. Chim. Acta* **1990**, *77*, 123. (b) Bergner, A.; Dolg, M.; Küchle, W.; Stoll, H.; Preuss, H. *Mol. Phys.* **1999**, *30*, 1431.

function ($\alpha = 1.235$ for f on Ru and $\alpha = 0.387$ for d on P). The atoms directly bonded to Ru (C, N, hydrides, and the ligands N_2, CO, C_2H_4, and O_2) were treated with 6-31G(d,p) basis sets, while the remaining atoms were represented with 6-31G basis sets. All the geometries were optimized without any symmetry constraint, and the natures of the extrema (minima or transition states) were checked by analytical computation of the Hessian matrixes. Unless otherwise stated, the energies given are electronic energies without any ZPE correction, as inclusion of the latter did not bring any significant alteration of the results.

Acknowledgment. This work was supported by the Deutsche Forschungsgemeinschaft, Bonn, Germany, the Fonds der Chemischen Industrie, the (DFH/UFA) Robert Bosch Stiftung, the University Montpellier 2, and the CNRS of France. We also thank the EU through the HCM program, Hydrogen Location and Transfer network.

Supporting Information Available: Tables giving X-ray structural data for **2**, **3**, **6,** and **8**. This material is available free of charge via the Internet at http://pubs.acs.org. CCDC 229177−229180 contain the supplementary crystallographic data for this paper. These data can be obtained free of charge via www.ccdc.cam.ac.uk/data_request/cif, by emailing data_request@ccdc.cam.ac.uk, or by contacting The Cambridge Crystallographic Data Centre, 12 Union Road, Cambridge CB2 1EZ, U.K. (fax +44 1223 336033).

OM034259C